Journal of Materials Chemistry A

Accepted Manuscript

ROYAL SOCIETY OF CHEMISTRY

www.rsc.org/materialsA

Journal Name

ARTICLE

An unprecedented anionic Ln-MOF with cage-within-cage motif: spontaneous reduction and immobilization of ion-exchanged Pd(II) to Pd-NPs in the framework

Received 00th January 20xx,
Accepted 00th January 20xx

DOI: 10.1039/x0xx00000x

www.rsc.org/

Yun-Hu Han,[a, b] Chong-Bin Tian,[a] Ping Lin[a] and Shao-Wu Du*[a]

An unprecedented microporous anionic Ln-MOF, $[Me_2NH_2]_{24}[Tb_{12}(TATB)_{16}(HCOO)_{12}]\cdot 12DMF\cdot 48H_2O$ (**1**) (H_3TATB = 4,4',4''-s-triazine-2,4,6-tribenzoic acid), which is a rare cage-within-cage structure through interpenetration rather than covalent bonds, has been synthesized. Compound **1** contains a 3D net which is constructed by a large and a small Ln-carboxylate cage alternately arranged by sharing faces with each other. Interpentration of two identical 3D net occurs in such a way that each samll cage of one net is encapsulated within the large cage of the other and *vise verse*, generating an overall 3D double-walled cage framework. Such interpenetration creates an unique structure of double-shelled hollow space to accommodate Pd nanoparticles (Pd-NPs), which could effectively prevent Pd-NPs from aggregation and leaching. Moreover, the ion-exchanged Pd(II) embedded in the framework can be readily reduced at room temperature with no requirement of any chemical or thermal treatments, affording Pd-NPs with uniform size and even distribution. As a result, the as-prepared **Pd-NPs@1** exhibits excellent activity and cycling stability for the hydrogenation of styrene and its derivatives.

Introduction

The synthesis of palladium nanoparticles (NPs) immobilized on porous supports has attracted extensive interest in heterogeneous catalysis.[1] The size, distribution and morphologies of NPs as well as the property of supports have important effects on the catalytic performance.[2] Generally, small particle size may result in a high surface-to-volume ratio and provide a large number of available active sites per unit area for reaction substrates. Therefore, much effort has been devoted to embedding palladium NPs into porous materials containing coordination groups that offer great potential for control of particle size and prevention of NPs aggregation.[3] In recent years, metal-organic frameworks (MOFs) with attractive architectures, large surface areas and tunable functional pores have attracted much attention and may be considered as the next generation of porous materials to load metal nano-particles (M-NPs) for heterogeneous catalysis.[4] According to the investigation, loading noble metals on MOFs still faces a number of challenges. One of the key challenges that need to be overcome is that the preparation of M-NPs@MOFs often requires the reduction of noble metal ions by hydrogen at the temperature higher than 200°C or by utilizing traditional strong redox regents such as $NaBH_4$.[5] However, compared to inorganic and organic porous materials, MOFs are normally less stable especially under hash reduction conditions.[6] Therefore, it is desirable to either synthesize MOFs with robust porous frameworks or seek a method to produce M-Ps within the pore space under mild conditions. In addition, MOFs constructed by anionic cages are better candidates for making M-NP@MOFs as the noble metal ions can enter the pore by ion-exchange, avoiding the interference of the anions from the metal salts.

Self-assembly of metal-organic coordination cages (MOCCs) with high symmetry, well-defined cavities, and various polyhedral geometries has led to a number of 3D cage-based MOFs, such as the well-known MILs, ZIFs, PCNs, NOTTs, HKUST-1, and so on.[7–12] These species display fascinating properties that make them excellent candidates for gas storage and separation, drug delivery, ion exchange, molecular sensor and catalysis.[13] Up to now, most of these cage-based MOFs are constructed by simply sharing vertexes, edges and faces of the neighbouring cages, or by cage catenane and interlocking.[14] In a very rare case, a cage-within-cage motif where one cage is entirely encapsulated by the other cage and the outer and inner cages are interconnected with covalent bonds has been observed.[15] However, to the best of our knowledge, cage-within-cage porous framework through interpenetration of two identical 3D nets has not been

[a] *State Key Laboratory of Structural Chemistry, Fujian Institute of Research on the Structure of Matter, Chinese Academy of Sciences, Fuzhou, Fujian 350002, P. R. China.*
[b] *Graduate University of Chinese Academy of Sciences, Bejing 100039, P. R. China.*
Electronic Supplementary Information (ESI) available: Experimental details, additional figures, UV-Vis, TGA, XRD, XPR and FT-IR results for the synthesized samples. See DOI: 10.1039/x0xx00000x

reported. Besides, there have been only a few examples of cage-based MOFs constructed by lanthanide ions.[16]

It has been reported recently that some MOFs, e.g. MOF-5 and $[Zn_{17}(thb)_{14}(\mu_4\text{-}O)_4(H_2O)(Me_2NH_2)]\cdot Me_2NH_2\cdot x$guest, can be employed to prepare M-NP@MOFs at mild conditions.[17] These types of MOFs are able to propel the charge transfer efficiently from the organic linkers to Zn_4O_{13} inorganic clusters and readily reduce Au^+, Ag^+, Pt^{2+} and other noble metal ions upon either UV irradiation or heating. The quantum dot (QD) behaviour of the Zn_4O_{13} inorganic clusters in these compounds is believed to be responsible for this self-redox ability.[18] However, until now, spontaneous reduction of Pd^{2+} ions to Pd-NPs in MOFs at room temperature without the help of any additional agents, which would be advantageous for catalytic application, has not been reported yet. In this contribution, we report a highly rare anionic cage-within-cage microporous MOF, $[Me_2NH_2]_{24}[Tb_{12}(TATB)_{16}(HCOO)_{12}]\cdot 12DMF\cdot 48H_2O$ (**1**) (H_3TATB = 4,4',4''-s-triazine-2,4,6-tribenzoic acid, Me = CH_3-), where each double-walled cage-within-cage motif contains forty-eight negative charge. This compound has a cage-within-cage structure formed through interpenetration of two identical 3D cage nets and is the second example of cage-MOFs based on lanthanide ions. Significantly, the ion-exchanged Pd^{2+} ions can be spontaneously reduced to metallic Pd by formate groups of the framework, affording well-dispersed Pd-NPs with small and narrow size distribution. Moreover, such spontaneous reduction process can be accelerated by slightly heating the Pd^{2+}-treated sample of **1** or soaking it in methanol.

Experimental section

General information

All reagents were commercially purchased and used without any further purification. The purity of all gases is 99.999%. The TGA were performed on a TGA/NETZSCH STA449C instrument heated from 40 to 800ºC under a nitrogen atmosphere at a heating rate of 10°C/min. Powder X-ray diffraction was recorded on a PANalytical X`pert PRO X-ray Diffraction using Cu-Kα radiation in the 2θ range of 5–50°. The Fourier transform infrared spectra using KBr pellets were collected on a Spectrum-One FT-IR spectrophotometer in the range of 4000–400 cm^{-1}. Elemental analyses (C, H, N) were measured with an Elemental Vairo EL III Analyser. Gas adsorption measurement was performed in the ASAP (Accelerated Surface Area and Porosimetry) 2020 System. All the Gas-chromatography (GC) measurements were analysed using a GC-Smart (SHIMADZU) with a DM-1 capillary column (L = 30 m; ID = 0.25 µm) and a flame ionization detector (FID). Analysis of noble metal content was measured by inductively coupled plasma atomic emission spectroscopy (ICP-AES) on an Ultima 2 analyser (Jobin Yvon). X-ray photoelectron spectra (XPS) was recorded by the Thermo Scientific *ESCALAB 250Xi* Spectrometer. ^{1}NMR spectra were recorded on a Bruker AVANCE III NMR spectrometer. Transmission electron microscopy (TEM) images were obtained with a TECNAI GzF20.

Preparation of $[Me_2NH_2]_{24}[Tb_{12}(TATB)_{16}(HCOO)_{12}]\cdot 12DMF\cdot 48H_2O$ (1)

A mixture of $Tb(NO_3)_3\cdot 6H_2O$ (0.50 mmol, 226.47 mg) and 4,4',4''-s-triazine-2,4,6-tribenzoic acid (H_3TATB, 0.5 mmol, 220.70 mg) was sealed in a 20 mL of Teflon-lined stainless steel vessel with 6 mL of dimethylformamide (DMF). The mixture was heated to 150 ºC in 4 hours and kept this temperature for 3 days. Then the reaction system was cooled slowly to room temperature during another 4 days. The colorless cubic crystals of **1** were collected, washed with DMF and acetonitrile and dried in air (yield 85% based on $Tb(NO_3)_3\cdot 6H_2O$). Elemental analysis calcd. (%) for $C_{480}H_{576}N_{72}O_{180}Tb_{12}$ (12141.31): C 47.48, H 4.78, N 8.31; found: C 47.19, H 4.73, N 8.19. IR (KBr, cm^{-1}): 3377s, 2978w, 2881w, 1629w, 1589w, 1541vs, 1427s, 1367vs, 1307w, 1172w, 1182w, 1089w, 1014w, 933vw, 879s, 831vs, 806s, 779s, 700w, 648w, 604w, 559s, 497w, 428w.

Single-crystal X-ray Diffraction Study

Single-crystal X-ray diffraction data were collected on a Rigaku Diffractometer with a Mercury CCD area detector (Mo Kα: λ = 0.71073 Å) at room temperature. Crystal Clear software was used for data reduction and empirical absorption correction. The structure was solved by direct method using SHELXTL and refined by full-matrix least-squares on F^2 using SHELX-97 program. Metal atoms in the compound were located from the *E*-maps, and other non-hydrogen atoms were located in successive difference Fourier syntheses. All non-hydrogen atoms were refined anisotropically. The organic hydrogen atoms were positioned geometrically. Because partial guest solvent molecules in channels were highly disordered and could not be modelled properly, thus the SQUEEZE routine of PLATON was applied to remove contributions to scattering from solvent molecules. The reported refinements are of guest-free structure by SQUEEZE routine. The final formulas of compounds were determined by combining with the results of the elemental analysis and thermogravimetric analysis. Crystallographic data and other pertinent information for **1** are summarized in Table S1. CCDC numbers for **1** is 1063756.

PXRD and TGA Measurement

In order to check the phase purity of the sample, the PXRD of the compound was recorded at room temperature. The peak positions of the simulated pattern closely match those of the experimental ones, indicating phase purity of the as-synthesized sample (Fig. S1). The TGA measurements were performed to study the thermal stability of **1** (Fig. S2). For fresh sample of **1**, the TGA curve does not show any platform from 40 to 400°C, which is due to the sustained loss of lattice solvent molecules, then the compound begins to decompose upon further heating till approximately 500°C. But, when we treat the sample at 150°C under vacuum for 24 hours, we can markedly see a platform appeared till nearly 250°C, indicating that the lattice solvent molecules can be largely removed at 150°C under vacuum for 24 hours.

Results and discussion

Colourless crystals of **1** were prepared under solvothermal conditions *via* the combination of $Tb(NO_3)_3{\cdot}6H_2O$ salt with the organic linker 4,4',4''-s-triazine-2,4,6-tribenzoic acid (H_3TATB) at 150°C in DMF. Single-crystal X-ray diffraction study reveals that **1** crystallizes in the cubic space group *Im*-3. The crystal structure is consisted of an anionic subjectival network and dimethylamine counter cations. The asymmetry unit of **1** is composed of one in four Tb^{3+} ion, one third $TATB^{3-}$ ligand, one fourth formic acid and half dimethylamine cations, which are derived from the decomposition of DMF. In the 3D anionic framework, the crystallographic independent Tb^{3+} ion adopts distorted enneahedral pyramidal coordination geometry, and is coordinated by nine-oxygen atoms, eight from four different $TATB^{3-}$ ligands while the rest one from formic acid (Fig. S3). The Tb–O bond lengths vary from 2.237(5) to 2.417(6) Å, which fall in a normal range for lanthanide carboxylate compounds.

The most fascinating topological feature of **1** is the highly rare cage-within-cage motif, in which the small cage is caged by a large cage (Fig. 1b), a result from the interpenetration of two independent but identical 3D cage nets (Fig. 1a). The small cage is constituted by twelve Tb^{3+} ions interconnected by eight $TATB^{3-}$ ligands and six formic acids, which defines an irregular cavity with a diameter of approximately 1.92 nm (Fig. 2d). Another twelve Tb^{3+} ions and eight $TATB^{3-}$ ligands form a large cage with a regular icosahedral geometry, whose diameter is up to 2.67 nm (Fig. 2e). Each small cage possesses twelve pentagonal windows, and the aperture of these windows is *ca.* 11.4 × 16.3 $Å^2$ (Fig. 1c). The large icosahedrons cage has six boat-windows, whose window size is about 26.7 × 19.9 $Å^2$ (Fig. 1c). The network topology of the structure analysed with the program package TOPOS is $\{6^3\}_8{\cdot}\{6^6{\cdot}8^4\}_6{\cdot}\{6\}_3$ net, which is a new topological type (Fig. S4). Further analysing the structure of **1** reveals that these two types of cages are alternatively arranged to form a 3D network in which each small cage is encircled by eight large cages (Fig. 2a), and each large cage is surrounded by eight small cages through the sharing of faces (Fig. 2b). Two identical 3D cage networks are interpenetrated in such a way that every small cage in one net is completely encapsulated by a large cage belonging to the other net and *vise verse*, resulted in a 3D net with double-walled cages (Fig. 2c).

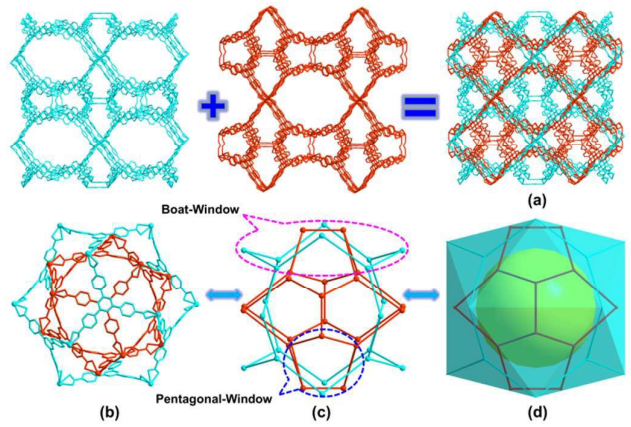

Fig.1 (a) Interpenetration of two identical 3D cage nets. (b, c, d) The cage-within-cage motif of **1**.

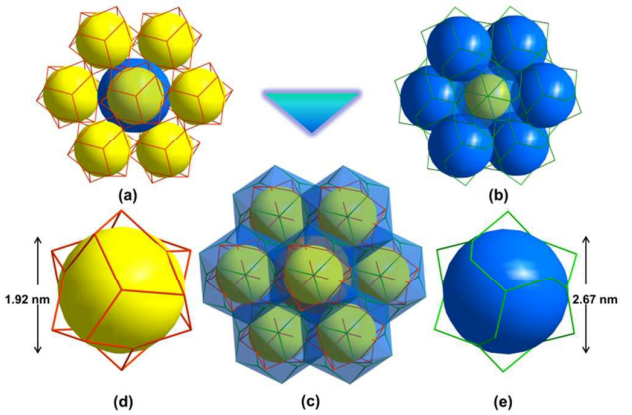

Fig. 2 (a, b) The large/small cage enriched by eight small/large cages. (c) Cage-within-cage motif resulted from the interpenetration of two identical 3D nets. (d, e) The approximate diameters of the small and large cages.

When the lattice solvent molecules, along with the counter cations in **1** are removed using SQUEEZE routine of PLATON, the PLATON/VOID calculation shows that the total empty volume of the anionic framework is 12464.1 $Å^3$, corresponding to 65.3 % of the total crystal volume (19090.7 $Å^3$). However, if only the lattice solvent molecules are removed, it decreases to 4167.5 $Å^3$, corresponding to 21.8 % of the total crystal volume. This result suggests that the void space of the framework is mainly filled with counter cations, which take up at least 43.5% of the total crystal volume. From the structure of **1**, we can see that every cage requires twenty-four $Me_2NH_2^+$ cations to balance the negative charges of the cage. In other words, each double-walled cage should contain forty-eight $Me_2NH_2^+$ cations inside the cavity for charge balance. The ^1H NMR spectrum of the acid-digested sample displays signals for $Me_2NH_2^+$ and $HCOO^-$ in a ratio of approximately 12:1, which is in agreement with the formula (Fig. S5b). It is expected that these $Me_2NH_2^+$ cations can be readily exchanged with noble metal ions and the anionic cage should be of benefit to the impregnation and immobilization of noble metal ions.

The phase purity of **1** was checked by PXRD recorded at room temperature. As illustrated in Fig. S3, the peak positions of the simulated pattern closely match those of the experimental ones, indicating phase purity of the as-synthesized sample. The TGA measurement was performed to study the thermal stability of **1** (Fig. S4). The TGA curve of **1** shows a continual weight loss without an obvious plateau from 40 to 500°C. After removing the lattice solvents by treating **1** under vacuum at 150°C for 24 hours, no obvious change was observed for the XRD (Fig. S3), indicating that **1** retains its structural integrity and crystallinity upon solvent removal. TGA curve of the desolvated sample shows no weight loss from 0 to *ca.* 250°C. After that the framework starts to decompose.

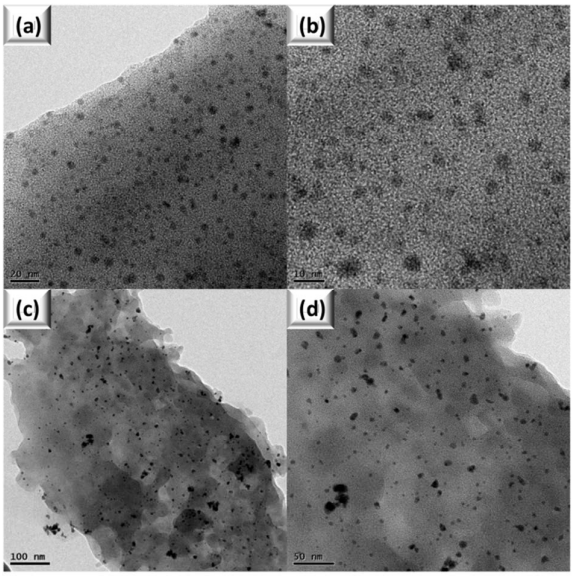

Fig. 3 The TEM images of **Pd-NPs@1** (a, b) and **Pd-NPs@1'** (c, d)

The $Me_2NH_2^+$ cations in solvent-free sample **1a** can perform ion-exchange with Pd^{2+} cations by soaking 500 mg colourless **1a** in a 20 mL 0.01 M THF solution of $Pd(NO_3)_2$. When the soaking experiment was conducted at room temperature, we found that some brown-black solid of metallic Pd was formed as confirmed by XPS (Fig. S6), which sticked to the surface of **1a** and confined further ion-exchange process. This result suggested that the Pd^{2+} ions can be facilely reduced to metallic Pd in the anionic framework of **1**. It can be speculated that the formate group in the framework may be responsible for the spontaneous reduction of Pd^{2+} ion to Pd.[19] After reduction, the intensity of the proton resonance attributed to fromate group is dramatically reduced in the ^{1}H NMR spectrum of the sample (Fig. S5d). The loss of formate anion did not result in the collapse of the subjectival framework, which was confirmed by XRD (Fig. S1). One way to avoid spontaneous reduction was to perform ion-exchange at low temperature. Thus, the orange-yellow Pd^{2+} embedded product **1b** could be successfully obtained by repeatedly soaking the sample in a 20 mL of fresh THF solution at –18°C every 24 h for one week. No metallic Pd was found in **1b** as evidenced by the XPS result (Fig. S6). The content of Pd^{2+} in **1b** determined by inductively coupled plasma atomic emission spectroscopy (ICP-AES) was 2.52 wt%. In comparison with other cases where the formation of Pd-NPs@MOFs usually required additional reducing agents, photoactivation or thermal energy, the reduction of Pd^{2+} to Pd-NPs in **1b** took place spontaneously and smoothly.

The direct preparation of Pd-NPs was achieved by simply treating **1b** under vacuum for four weeks at room temperature. However, the size of Pd-NPs obtained by this procedure was too small and incomplete reduction of Pd^{2+} ions was observed (Fig. S7 and S8). In order to accelerate the reduction of Pd^{2+}, we carried out the experiment at 80°C for one hour, which led to the complete reduction of Pd^{2+} ions and afforded bigger Pd-NPs in **1** (denoted as **Pd-NPs@1**) with good uniform size and even distribution (Fig. 3a, b). We found that it was also possible to speed up the reduction of Pd^{2+} ions by soaking **1b** in methanol. After 24 hours, Pd-NPs with relatively poor dispersion and distribution compared to those obtained at 80°C were formed in the framework of **1** (denoted as **Pd-NPs@1'**) (Fig. 3c, d). The generation of metallic Pd in the Pd-NPs loading sample **Pd-NPs@1** is visible with a colour change from orange-yellow to dark brown-black (Fig. S9). By extending the soaking time using solution with a high concentration of $Pd(NO_3)_2$, the content of Pd^{2+} can reach to a maximum of 12.67 wt%, affording ion-exchange sample **1c**. The ^{1}H NMR spectrum of **1c** shows almost no residual signal for the methyl proton of $Me_2NH_2^+$, indicating complete replacement of $Me_2NH_2^+$ by Pd^{2+} (Fig. S5c). As expected, reduction of Pd^{2+} in **1c** afforded **Pd-NPs@1c** with bigger and more densely packed Pd-NPs compared to **Pd-NPs@1** and **Pd-NPs@1'** (Fig. S10).

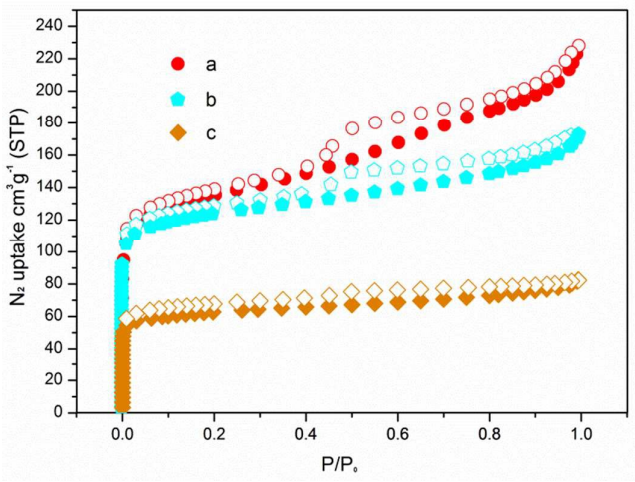

Fig. 4 The nitrogen adsorption for (a) **1c**, (b) **Pd-NPs@1c**, and (c) **1a**.

The N_2 adsorption measurements of **1a** and **1c** are also recorded. Because the cavities of **1a** is filled with $Me_2NH_2^+$ cation, when **1a** is ion-exchanged with Pd^{2+}, the N_2 adsorption capacity would be expected to increase. The N_2 adsorption measurements verified this point, giving Langmuir and BET surface areas of 284 and 200 m^2g^{-1} for **1a** and 627 and 447 m^2g^{-1} for **1c** (Fig. 4a, c). The permanent porosity of **Pd-NPs@1c** is also proved by N_2 adsorption measurement, which gives 565 and 398 m^2g^{-1} for Langmuir and BET surface areas (Fig. 4b). The total pore volumes of **1a, 1c** and **Pd-NPs@1c** obtained from the N_2 adsorption isotherms recorded at 77 K are 0.13 0.33 and 0.27 cm^3g^{-1}, respectively. The experimental value of **1a** is less than 0.23 cm^3g^{-1} calculated by using the accessible volume from PLATON and the unit cell mass. This is either because of the incomplete removal of solvent molecules from the sample, or the slight porosity loss during the activated process. No characteristic peaks of Pd metal appeared in the XRD pattern of **Pd-NPs@1c** due to the little amount of Pd-NPs compared to that of the host solid (Fig. S1). It also indicated that small-sized Pd-NPs were well dispersed throughout the MOF support.

The existing state of the surface palladium was investigated by XPS. In the XPS spectrum of the Pd^{2+}-embedded sample prepared at room temperature, the Pd 3d region is divided into two spin-orbital pairs, indicating the presence of two types of surface-bound palladium species (Fig. S6). The binding energy peaks at 343.38 (Pd $3d_{5/2}$) and 338.18 eV (Pd $3d_{3/2}$) are assigned to Pd^{2+} species, while the small peaks at 340.98 (Pd $3d_{5/2}$) and 335.88 eV (Pd $3d_{3/2}$) correspond to metallic Pd species, which is probably resulted from the spontaneous reduction of Pd^{2+} by the anionic framework. When the sample was prepared at –18°C, only peaks related to Pd^{2+} were observed (Fig. S6). The XPS spectrum of **Pd-NPs@1** exhibits only two peaks for metallic Pd, indicating complete reduction of Pd^{2+} to Pd-NPs (Fig. S8). In contrast, considerable amount of Pd^{2+} remains unreduced in **Pd-NPs@1'**, as can be seen from Fig. S11. Transmission electron microscopy (TEM) images reveal that the average diameter of Pd-NPs is 4.28 ± 0.21 nm for **Pd-NPs@1** and 9.12 ± 0.32 nm for **Pd-NPs@1'**, showing a narrow distribution. These Pd-NPs are a little larger than some other immobilized Pd-NPs in organic-inorganic hybrid materials.[20]

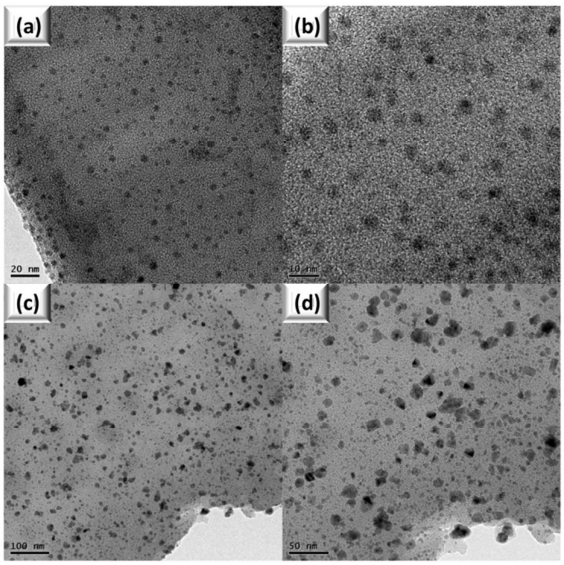

Fig. 5 The TEM images of the catalysts after six runs for **Pd-NPs@1** (a, b) and **Pd-NPs@1'** (c, d).

The catalytic performance of **Pd-NPs@1** and **Pd-NPs@1'** was evaluated *via* the hydrogenation of styrene and its derivatives at room temperature. In a typical reaction, 5 mg of **Pd-NPs@1** (2.52 wt%) was used for the conversion of 2 mmol of styrene, and the reaction was carried out under 1 atm of hydrogen in THF at room temperature. The conversion of styrene was determined by gas chromatography (GC). The conversion of styrene to ethylbenzene is completed in 7 hours with **NPsPd@1**, and 8.5 hours with **NPsPd@1'**, giving 100% yield of the hydrogenation product. The catalytic activity of both catalysts is better than other Pd-NPs@MOFs but is comparable to that for Pd-NPs@MIL-101 and Pd-NPs@MOF-5, which require 7 and 12 hours respectively to complete the hydrogenation.[21] Notably, a 100% conversion of styrene to ethylbenzene can be achieved within one hour when the temperature of hydrogenation was increased to 60°C. During the catalytic reaction, the H_2 and olefin are attached to the surface of Pd-NPs. First, the H-H bond in H_2 cleaves to generate two Pd-H bonds. Then both hydrogen atoms are added across the double bond of an alkene, resulting in a saturated alkane (Scheme S1).

In addition to high catalytic activity, the reusability and stability are also very important for heterogeneous catalytic systems. The recycling experiments were conducted using **Pd-NPs@1** and **Pd-NPs@1'** as catalysts in the hydrogenation of styrene without the addition of extra palladium. The results indicated that no obvious efficiency loss was detected after six runs. However, in the case of **Pd-NPs@1'**, after six runs, increasing catalytic activity was observed. We speculated that the unreduced Pd^{2+} ions in **Pd-NPs@1'** were continuingly reduced during the hydrogenation reaction to afford more Pd-NPs. This is in agreement with the XPS results where two peaks belonging to Pd^{2+} ions after six runs are noticeably reduced compared to those before the reaction (Fig. S11). As shown Fig. 5, the TEM image reveals that the granular particles of both catalysts are well maintained after six consecutive runs, with the average of diameter being slightly increased to 4.29 ± 0.31 nm for **Pd-NPs@1** and 9.4 ± 0.6 nm for **Pd-NPs@1'**, and no obvious aggregation of Pd-NPs was observed. However, in the case of **Pd-NPs@1'**, the density of Pd-NPs was increased, indicating again that additional Pd^{2+} ions were reduced after catalytic reactions.

Leaching experiment was performed to examine the stability of the Pd-NPs. After the first run, ICP analysis showed that the amount of palladium leached out into the solvent was only 12 ppb for **Pd-NPs@1** and 16 ppb for **Pd-NPs@1'**. Besides, after three hours when the conversion yield reached 57.3%, the catalyst was removed from the solution and the reaction was continued for three hours, the conversion of styrene to ethylbenzene remained unchanged as checked by GC (Fig. S12), implying that there was no contribution from palladium leached into reaction solution. We believe that the unique structure of **1** can effectively prevents the aggregation and leaching of Pd-NPs and increase their catalytic active area, and hence enhance their stability and catalytic performance. Moreover, the interaction of nitrogen atoms from the $TATB^{3-}$ ligand with Pd-NPs may also help stabilize a dispersion of the nanoparticles.

The excellent catalytic activity of **Pd-NPs@1** encouraged us to further explore the generality of this catalytic system. Further tests using some styrene derivatives with different electronic and steric characters were investigated (Table 1). For easy comparison, all the experiments were performed under the same conditions. The substrates carrying electron-donating groups in the *para* positon, such as methyl, methoxy or *tert*-butyl resulted in total conversion to the corresponding hydrogenated products (Entry 1–3). Halogenated styrenes provided a full conversion, and the substituted position (*meta* or *para*) had no influence on the activity (Entry 4–7). Substrate with a methylvinyl group gave 87% conversion whereas that with a nitrovinyl group led to no hydrogenated product (Entry 8, 9). Bulky substituents on the vinyl group dramatically reduced the catalytic activity of **Pd-NPs@1** (Entry 10) and for

tetraphenylethene, no product was obtained (Entry 11). The framework of **1** has no activity in the hydrogenation of styrene (Entry 12).

Table 1 Hydrogenation of styrene and its derivatives

Entry	Substrates	Products	Conv. (%)[a]
1	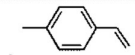	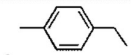	100
2	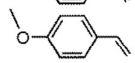	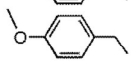	100
3	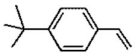	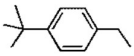	98
4	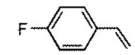	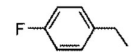	100
5	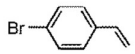	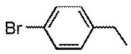	100
6	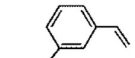	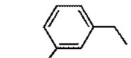	99
7	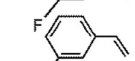	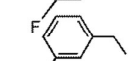	98
8	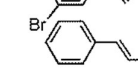	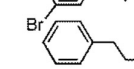	87
9	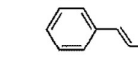	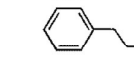	0
10	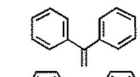	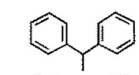	12
11	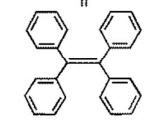	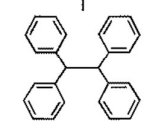	0
12[b]	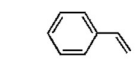	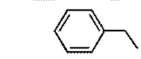	0

[a] Reaction conditions: olefin (2 mmol), H_2 1atm and [Pd] (0.06 mmol%), in 2.5 mL THF at room temperature for 7 hours. Conversion was determined by GC. [b] Hydrogenation of styrene with **1** as catalyst.

Conclusions

In summary, we have synthesized an anionic Ln-MOF with an unprecedented double-walled cage motif. It is a rare cage-within-cage structure generated from interpenetration of two identical 3D cage nets and the second example of coordination cage based on lanthanide ions. Interestingly, the formate group of the framework can readily reduce Pd^{2+} ions without loss of the framework integrity, generating Pd-NPs with small particle size and narrow size distribution at room temperature without the help of any additional chemical or thermal treatments. Furthermore, such a reduction process can be accelerated via slightly heating or soaking the Pd^{2+}-treated sample in methanol. Owing to the efficient stabilization by the double-walled cages, the Pd-NPs with controlled size can be dispersed well onto **1**. The resultant **Pd-NPs@1** has exhibited high activity in the hydrogenation of olefins and it can be used up to six times without significant loss of the catalytic activity, showing a satisfactory reusability.

Acknowledgements

We thank the National Basic Research Program of China (973 Program, 2012CB821702), the National Natural Science Foundation of China (21233009, 21173221 and 21571175) and the State Key Laboratory of Structural Chemistry, Fujian Institute of Research on the Structure of Matter, Chinese Academy of Sciences for financial support.

Notes and references

1 (a) L. Liu, H. Zhao, J. Wang and R. Wang, *ACS Nano*, 2014, **8**, 5352; (b) Z. Li, J. Liu, C. Xia and F. Li, *ACS Catal.*, 2013, **3**, 2440; (c) A. Balanta, C. Godard and C. Claver, *Chem. Soc. Rev.*, 2011, **40**, 4973; (d) M. Lamblin, L. Nassar-Hardy, J. C. Hierso, E. Fouquet and F. X. Felpin, *Adv. Synth. Catal.*, 2010, **352**, 33; (e) R. Schlogl and S. B. Abd Hamid, *Angew. Chem., Int. Ed.*, 2004, **43**, 1628.

2 C. Burda, X. Chen, R. Narayanan, M. A. El-Sayed, *Chem. Rev.*, 2005, **105**, 1025.

3 (a) A. Dhakshinamoorthy and H. Garcia, *Chem. Soc. Rev.*, 2012, **41**, 5262; (b) L. Wang, S. Shylesh, D. Dehe, T. Philippi, G. Dörr, A. Seifert, Z. Zhou, M. Hartmann, R. N. Klupp Taylor, M. Jia, S. Ernst and W. R. Thiel, *ChemCatChem,* 2012, **4**, 395; (c) J. Li, X. Y. Shi, Y. Y. Bi, J. F. Wei and Z. G. Chen, *ACS Catal.*, 2011, **1**, 657.

4 (a) J. Liu, L. Chen, H. Cui, J. Zhang, L. Zhang and C. Su, *Chem. Soc. Rev.*, 2014, **43**, 6011; (b) X. Li, Z. Guo, C. Xiao, T. Goh, D. Tesfagaber and W. Huang, *ACS Catal.,* 2014, **4**, 3490; (c) A. Dhakshinamoorthy and H. Garcia, *Chem. Soc. Rev.*, 2012, **41**, 5262; (d) A. Dhakshinamoorthy, M. Alvaro and H. Garcia, *Catal.Sci.Technol.*, 2011, **1**, 856; (e) H. Jiang and Q. Xu, *Chem. Commun.*, 2011, **47**, 3351; (f) R. J. T. Houk, B. W. Jacobs, F. E. Gabaly, N. N. Chang, A. A. Talin, D. D. Graham, S. D. House, I. M. Robertson and M. D. Allendorf, *Nano Lett.*, 2009, **9**, 3413.

5 (a) T. Dang, Y. Zhu, J. S. Y. Ngiam, S. C. Ghosh, A. Chen and A. M. Seayad, *ACS Catal.*, 2013, **3**, 1406; (b) D. W. Lim, J. Yoon, K. Y. Ryu and M. P. Suh, *Angew. Chem., Int. Ed.*, 2012, **51**, 9814; (c) L. B. Vilhelmsen, K. S. Walton and D. S. Sholl, *J. Am. Chem. Soc.*, 2012, **134**, 12807; (d) H. Jiang, B. Liu, T. Akita, M. Haruta, H. Sakurai and Q. Xu, *J. Am. Chem. Soc.*, 2009, **131**, 11302.

6 (a) V. Pascanu, P. R. Hansen, A. B. Gómez, C. Ayats, A. E. Ayats-Prats, M. J. Johansson, M. Pericàs and B. Martín-Matute, *ChemSusChem* 2015, **8**, 123; (b) L. Shen, W. Wu, R. Liang, R. Lin and L. Wu, *Nanoscale*, 2013, **5**, 9374; (c) G. Lu, S. Li, Z. Guo, O. K. Farha, B. G. Hauser, X. Qi, Y. Wang, X. Wang, S. Han, X. Liu, J. S. DuChene, H. Zhang, Q. Zhang, X. Chen, J. Ma, S. C. Joachim Loo, W. Wei, Y. Yang, J. T. Hupp and F. Huo, *Nature Chemistry*, 2012, **4**, 310.

7 G. Férey, C. Mellot Draznieks, C. Serre, F. Millange, J. Dutour, S. Surblé, I. Margiolaki, *Science*, 2005, **309**, 2040.

8 K. S. Park, Z. Ni, A. P. Côté, J. Y. Choi, R. Huang, F. J. Uribe Romo, H. K. Chae, M. O'Keeffe, O. M. Yaghi, *PNAS*, 2006, **103**, 10186.

9 S. Ma, D. Sun, J. M. Simmons, C. D. Collier, D. Yuan, H. C. Zhou, *J. Am. Chem. Soc.*, 2008, **130**, 1012.

10 X. Lin, I. Telepeni, A. J. Blake, A. Dailly, C. M. Brown, J. M. Simmons, M. Zoppi, G. S. Walker, K. M. Thomas, T. J. Mays, P. Hubberstey, N. R. Champness, M. Schröder, *J. Am. Chem. Soc.*, 2009, **131**, 2159.

11 S. Y. Chui, S. M. F. Lo, J. P. H. Charmant, A. G. Orpen, I. D. Williams, *Science*, 1999, **283**, 1148.

12 H. Furukawa, N. Ko, Y. B. Go, N. Aratani, S. B. Choi, E. Choi, A. Ö. Yazaydin, R. Q. Snurr, M. O'Keeffe, J. Kim, O. M. Yaghi, *Science*, 2010, **329**, 424.

13 (a) R. J. Kuppler, D. J. Timmons, Q. R. Fang, J. R. Li, T. A. Makal, M. D. Young, D. Yuan, D. Zhao, W. Zhuang, H. C. Zhou, *Coord*. *Chem*. *Rev*., 2009, **253**, 3042; (b) C. Y. Sun , C. Qin, C. G. Wang, Z. M. Su, S. Wang, X. L. Wang, G. S. Yang, K. Z. Shao, Y. Q. Lan, E. B. Wang, *Adv. Mater.*, 2011, **23**, 5629; (c) C. Wang, D. Liu, W. Lin, *J*. *Am*. *Chem*. *Soc*., 2013, **135**, 13222; (d) Y. Chen, V. Lykourinou, C. Vetromile, T. Hoang, L. J. Ming, R. W. Larsen, S. Ma, *J*. *Am*. *Chem*. *Soc*., 2013, **135**, 13222; (e) X. T. Rao, T. Song, J. K. Gao, Y. J. Cui, Y. Yang, C. D. Wu, B. L. Chen and G. D. Qian, *J. Am. Chem. Soc.*, 2013, **135**, 15559.

14 (a) X. Kuang, X. Wu, R. Yu, J. P. Donahue, J. Huang, C. Z. Lu, *Nat*. *Chem*., 2010, **2**, 461; (b) J. Heine, J. Schmedt auf der Günne, S. Dehnen, *J*. *Am*. *Chem*. *Soc*., 2011, **133**, 10018; (c) L. Jiang, P. Ju, X. R. Meng, X. J. Kuang, T. B. Lu, *Sci*. *Rep*., 2012, **2**, 668.

15 S. T. Zheng, T. Wu, B. Irfanoglu, F. Zuo, P. Feng, X. Bu, *Angew*. *Chem*. *Int*. *Ed*., 2011, **50**, 8034.

16 (a) S. Ma, X. S. Wang, D. Yuan, H. C. Zhou, *Angew*. *Chem*. *Int*. *Ed*., 2008, **47**, 4130; (b) V. Guillerm, Ł. J. Weseliński, Y. Belmabkhout, A. J. Cairns, V. D'Elia, Ł. Wojtas, K. Adil and M. Eddaoudi, *Nat. Chem.,* 2014, **6**, 673.

17 (a) R. Ameloot, M. B. J. Roeffaers, G. D. Cremer, F. Vermoortele, J. Hofkens, B. F. Sels and D. E. De Vos, *Adv. Mater.*, 2011, **23**, 1788; (b) Y. Tan, Y. He and J. Zhang, *Chem. Commun.*, 2014, **50**, 6153.

18 (a) R. Ameloot, M. B. J. Roeffaers, G. D. Cremer, F. Vermoortele, J. Hofkens, B. F. Sels and D. E. De Vos, *Adv. Mater.*, 2011, **23**, 1788; (b) T. Tachikawa, J. R. Choi, M. Fujitsuka and T. Majima, *J. Phys. Chem. C*, 2008, **112**, 14090; (c) M. Alvaro, E. Carbonell, B. Ferrer, F. Xamena and H. Garcia, *Chem.-Eur. J.*, 2007, **13**, 5106; (d) S. Bordiga, C. Lamberti, G. Ricchiardi, L. Regli, F. Bonino, A. Damin, M. Bjorgenb and A. Zecchina, *Chem. Commun.*, 2004, 2300.

19 (a) H. W. Gibson, *Chem. Rev.*, 1969, **69**, 673, (b) M. Yadav, Q. Xu, *Chem. Commun.,* 2013, **49**, 3327, (c) K. N. Gong, W. J. Wang, J. S. Yan and Z. G. Han, J. Mater. Chem. A, 2015, **3**, 6019.

20 (a) A. Aijaz, Q. L. Zhu, N. Tsumori, T. Akita and Q. Xu, *Chem. Commun.*, 2015, **51**, 2577; (b) L. Y. Chen, H. R. Chen and Y. W. Li, *Chem. Commun.*, 2014, **50**, 14752; (c) L. Y. Chen, H. R. Chen R. Luque and Y. W. Li, *Chem. Sci.*, 2014, **5**, 3708.

21 A. Henschel, K. Gedrich, R. Kraehnert and S. Kaskel, *Chem. Commun.*, 2008, 4192.

Table of Contents

An unprecedented anionic Ln-MOF with cage-within-cage motif: spontaneous reduction and immobilization of ion-exchanged Pd(II) to Pd-NPs in the framework

Yun-Hu Han,[a, b] Chong-Bin Tian,[a] Ping Lin[a] and Shao-Wu Du*[a]

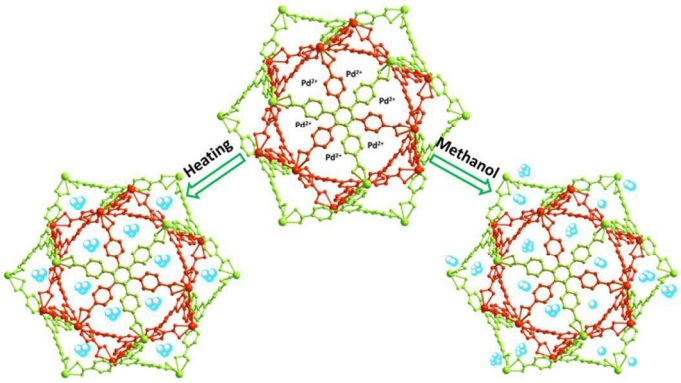

A first Ln-MOF with cage-within-cage motif was synthesized. Well-dispersed Pd-NPs embedded in the framework exhibits excellent activity for hydrogenation of styrene.